JVI Journals.ASM.org

Regulation of Hepatitis B Virus Infection by Rab5, Rab7, and the Endolysosomal Compartment

Alina Macovei,[a] Catalina Petrareanu,[a,b] Catalin Lazar,[a] Paula Florian,[c] Norica Branza-Nichita[a]

Institute of Biochemistry, Department of Viral Glycoproteins, Bucharest, Romania[a]; Department of Analytical Chemistry and Environmental Engineering, Faculty of Applied Chemistry and Materials Science, Polytehnica University of Bucharest, Bucharest, Romania[b]; Institute of Biochemistry, Department of Ligand-Receptor Interactions, Bucharest, Romania[c]

Despite important progress toward deciphering human hepatitis B virus (HBV) entry into host cells, many aspects of the early steps of the life cycle remained completely obscure. Following endocytosis, HBV must travel through the complex network of the endocytic pathway to reach the cell nucleus and initiate replication. In addition to guiding the viral particles to the replication site, the endosomal vesicles may play a crucial role in infection, providing the appropriate environment for virus uncoating and nucleocapsid release. In this work, we investigated the trafficking of HBV particles internalized in permissive cells. Expression of key Rab proteins, involved in specific pathways leading to different intracellular locations, was modulated in HepaRG cells, using a stable and inducible short hairpin RNA (shRNA) expression system. The trafficking properties of the newly developed cells were demonstrated by confocal microscopy and flow cytometry using specific markers. The results showed that HBV infection strongly depends on Rab5 and Rab7 expression, indicating that HBV transport from early to mature endosomes is required for a step in the viral life cycle. This may involve reduction of disulfide bond-linked envelope proteins, as alteration of the redox potential of the endocytic pathway resulted in inhibition of infection. Subcellular fractionation of HBV-infected cells showed that viral particles are further transported to lysosomes. Intriguingly, infection was not dependent on the lysosomal activity, suggesting that trafficking to this compartment is a "dead-end" route. Together, these data add to our understanding of the HBV-host cell interactions controlling the early stages of infection.

Chronic hepatitis B virus (HBV) infections can lead to life-threatening liver diseases, such as cirrhosis and hepatocellular carcinoma, the third cause of cancer deaths worldwide (1). Infectious viral particles consist of an icosahedral nucleocapsid made of the core protein and a lipid bilayer embedding the small (S), middle (M), and large (L) envelope proteins (2). The nucleocapsid surrounds the relaxed circular, partially double-stranded DNA genome, to which the viral polymerase is covalently attached (3). Apart from the crucial roles played in virus morphogenesis and infection, the envelope proteins bear the intriguing property to self-assemble into spherical and filamentous subviral particles (SVP), which are released from cells in vast excess over virions, accounting for more than 90% of the total particles in the serum of infected patients (4).

Studies regarding the early events of the HBV life cycle have been particularly problematic, as human primary hepatocytes, the physiological host, are difficult to procure and maintain in tissue culture and are refractory to genetic manipulation. The development of alternative infectivity models for HBV, represented by proliferating liver-derived cell lines able to differentiate and support HBV infection *in vitro*, has considerably overcome many of these drawbacks (5–7). Moreover, the suitability of differentiated umbilical cord matrix stem cells to investigate the early steps of HBV infection was also demonstrated (8). Thus, important progress in understanding viral entry has been made within the last years; the molecular determinants of HBV attachment to target cells have been characterized for both host cells (9, 10) and the viral particle (11), and new cellular factors such as caveolin-1, clathrin heavy chain, and clathrin adaptor protein AP-2 have been described to play a role in HBV endocytosis in different cell lines (6, 12). Very recently, sodium taurocholate cotransporting polypeptide (NTCP), a multiple-domain-spanning transmembrane transporter, has been proposed as a functional receptor for HBV and hepatitis D virus (HDV) (13). Following cell attachment and endocytosis, virus particles must travel along the endocytic route to reach the replication site. Despite these recent discoveries, the intracellular trafficking events, which are critical for the initiation of a productive infection by providing the appropriate environment for virus uncoating and nucleocapsid release, have remained completely obscure for HBV.

The dynamics of the complex network of vesicles of the endocytic pathway is regulated by Rab proteins and their effectors (14). These are small guanosine triphosphatases (GTPases) of the Ras superfamily involved in selection of vesicle cargos, budding, targeting, and fusion (15–17). Owing to a restricted expression pattern in specific endocytic compartments and their ability to recruit distinctive effector proteins, Rab proteins are powerful tools to discriminate between pathways leading to different intracellular locations (16, 18, 19).

In this work we investigated the trafficking of HBV particles at postentry stages, by modulating expression of endogenous Rab5, Rab7, Rab9, and Rab11 in differentiated HepaRG cells, which are permissive for HBV infection. These proteins regulate individual steps in the transport of newly endocytosed vesicles, from the plasma membrane to early endosomes (Rab5) (20) and further to late endosomes and lysosomes (Rab7) (21) or the *trans*-Golgi net-

Received 11 February 2013 **Accepted** 21 March 2013
Published ahead of print 27 March 2013
Address correspondence to Norica Branza-Nichita, nichita@biochim.ro.

doi:10.1128/JVI.00393-13

TABLE 1 Short hairpin oligonucleotide sequences used for Rab5, Rab7, Rab9, and Rab11 depletion

Protein	Sequence no.	Sequence order	Sequence
Rab5	1	Top	5′ CACCGCAGCCATAGTTGTATATGATGAGAATCATATACAACTATGGCTGC 3′
		Bottom	5′ AAAAGCAGCCATAGTTGTATATGATTCTCATCATATACAACTATGGCTGC 3′
	2	Top	5′ CACCGGAATCAGTGTTGTAGTAACTGAGAAGTTACTACAACACTGATTCC 3′
		Bottom	5′ AAAAGGAATCAGTGTTGTAGTAACTTCTCAGTTACTACAACACTGATTCC 3′
Rab7	1	Top	5′ CACCGGAAGACATCACTCATGAACCGAGAGGTTCATGAGTGATGTCTTCC 3′
		Bottom	5′ AAAAGGAAGACATCACTCATGAACCTCTCGGTTCATGAGTGATGTCTTCC 3′
	2	Top	5′ CACCGCTAGTCACAATGCAGATATGGAGACATATCTGCATTGTGACTAGC 3′
		Bottom	5′ AAAAGCTAGTCACAATGCAGATATGTCTCCATATCTGCATTGTGACTAGC 3′
Rab9	1	Top	5′ CACCGGTGGAGTTGGGAAGAGTTCAGAGATGAACTCTTCCCAACTCCACC 3′
		Bottom	5′ AAAAGGTGGAGTTGGGAAGAGTTCATCTCTGAACTCTTCCCAACTCCACC 3′
	2	Top	5′ CACCGGTAACAAGATTGACATAAGCGAGAGCTTATGTCAATCTTGTTACC 3′
		Bottom	5′ AAAAGGTAACAAGATTGACATAAGCTCTCGCTTATGTCAATCTTGTTACC 3′
Rab11	1	Top	5′ CACCGGAGATTCTGGTGTTGGAAAGGAGACTTTCCAACACCAGAATCTCC 3′
		Bottom	5′ AAAAGGAGATTCTGGTGTTGGAAAGTCTCCTTTCCAACACCAGAATCTCC 3′
	2	Top	5′ CACCGCAACAATGTGGTTCCTATTCGAGAGAATAGGAACCACATTGTTGC 3′
		Bottom	5′ AAAAGCAACAATGTGGTTCCTATTCTCTCGAATAGGAACCACATTGTTGC 3′

work (Rab9) (22) and are also involved in vesicle recycling (Rab11) (23, 24). We demonstrate that silencing of either Rab5 or Rab7 expression results in significant inhibition of the early stages of HBV infection, while Rab9 and Rab11 have no effect. The results indicate that transport of viral particles to late endosomes is required for a crucial step of the life cycle, most probably the nucleocapsid release. Subcellular fractionation of HBV-infected cells showed that an important amount of viral particles are further transported to late endosomes/endolysosomes, in a time-dependent manner. Intriguingly, interference with the lysosomal activity by pH neutralization or treatment with protease inhibitors had no effect on infection, suggesting that HBV transport into the degradative branch of the endocytic pathway is not required to initiate this process. Together, these data build up a model for the cellular mechanisms of HBV trafficking controlling the early stages of the viral life cycle.

MATERIALS AND METHODS

Cell lines. HepaRG cells were routinely maintained in William's E medium (Gibco) supplemented with 10% fetal bovine serum, 50 U/ml penicillin, 50 μg/ml streptomycin, 2 mM Glutamax (Invitrogen), 5 μg/ml insulin, and 5×10^5 M hydrocortisone hemisuccinate (Sigma). Cell differentiation was induced by addition of 2% dimethyl sulfoxide (DMSO) to the medium, as previously described (5). HepG2.2.2.15 cells, stably transfected with two copies of the HBV genome, were grown in RPMI 1640 medium (Euroclone) containing 10% fetal bovine serum (FBS), 50 U/ml penicillin, 50 μg/ml streptomycin, and 2 mM Glutamax (Invitrogen), supplemented with 200 μg/ml of G418 (Gibco).

Generation of HepaRG cell lines stably expressing tetracycline-inducible short hairpin RNA (shRNA) specific for Rab5, Rab7, Rab9, and Rab11. All short hairpin oligonucleotide sequences (Invitrogen) (Table 1) were cloned into pENTR/H1/TO entry vector (Invitrogen) following the manufacturer's instructions, and the correct insertion was confirmed by sequencing. Of the three known Rab5 isoforms, Rab5a was targeted for silencing, due to its ubiquitous expression and established function in regulating trafficking through the early endocytic pathway. The shRNA expression vector pLenti4/H1/TO was generated by recombination pENTR/H1/TO entry vector with the pLenti4/BLOCK-iT-DEST vector via a standard Gateway LR recombination reaction (Invitrogen). The plasmid confers zeocin resistance and expression is controlled by a tetracycline (Tet)-regulated promoter.

The HepaRG^{tetR} cell line stably overexpressing the Tet repressor (tetR) was obtained by transduction with a lentivirus produced from pLenti6-TR plasmid (BLOCK-iT inducible H1 lentiviral RNA interference [RNAi] system; Invitrogen). Transduced cells were treated with 2 μg/ml blasticidin S, and resistant clones were selected following serial dilution. HepaRG^{tetR} cells were transduced with the pLenti4/H1/TO lentivirus containing a specific shRNA sequence, cloned above. HepaRG clones expressing shRNA specific for Rab5 (HepaRG$^{tetR/shRab5}$), Rab7 (HepaRG$^{tetR/shRab7}$), Rab9 (HepaRG$^{tetR/shRab9}$), and Rab11 (HepaRG$^{tetR/shRab11}$) were selected by serial dilution in the presence of 400 μg/ml zeocin. In control experiments, HepG2.2.2.15$^{tetR/shRab5}$ and HepG2.2.2.15$^{tetR/shRab7}$ cell lines were also generated following the same procedure as described for HepaRG. For further maintenance and induction experiments, the new cell lines were grown in their corresponding medium supplemented with 1 μg/ml blasticidin S and 200 μg/ml zeocin.

SDS-PAGE and Western blotting. Cells were grown in six-well plates, and shRNA expression was induced with 1 μg/ml Tet for 72 h. Cells were further lysed as described previously (25), and lysates were subjected to centrifugation at 10,000 × *g* for 10 min. The proteins in the supernatant were quantified using the bicinchoninic acid method (Pierce), and equal amounts were loaded for sodium dodecyl sulfate-polyacrylamide gel electrophoresis (SDS-PAGE). The proteins were transferred to nitrocellulose membranes using a semidry blotter (Millipore) and detected by incubation with either rabbit anti-Rab5, -Rab7, and -Rab9 antibodies (Abs) (Cell Signaling Technology, diluted 1:1,000) or mouse anti-Rab11 antibody (BD Transduction Laboratories, diluted 1:1,000) followed by horseradish

peroxidase (HRP)-conjugated goat anti-rabbit (Cell Signaling Technology, diluted 1:2,000) or sheep anti-mouse (GE Healthcare, diluted 1:2,000) Abs. Detection of calreticulin (Crt) expression with goat anti-Crt (Santa Cruz Biotechnology, diluted 1:500) followed by donkey anti-goat HRP-conjugated Abs (Santa Cruz Biotechnology, diluted 1:200) was used as a control. The proteins were visualized using the ECL enhanced chemiluminescence detection system (GE Healthcare).

Confocal fluorescence microscopy. Cells were seeded on cover glass and maintained for 3 days in the presence or absence of 1 μg/ml Tet. When human transferrin (hTfn) internalization was monitored, the cells were washed with phosphate-buffered saline (PBS) and incubated for 1 h in serum-free medium before addition of 50 μg/ml hTfn-Alexa Fluor 488 (Invitrogen), for 30 min at 4°C. The medium containing the fluorescent marker was removed, and the cells were washed three times with PBS, followed by 30-min incubation in complete medium at 37°C. For microscopy analysis cells were fixed with 4% paraformaldehyde, washed three times with PBS, permeabilized with 0.2% Triton X-100 in PBS, and incubated for 30 min with specific primary Abs. Rabbit anti-Rab5, -Rab7, and -Rab9 or mouse anti-Rab11 was used at a 1:100 dilution. Mouse anti-Lamp1 (Santa Cruz Biotechnology) and cation-independent mannose 6-phosphate receptors (CI-MPRs) (Santa Cruz Biotechnology) were diluted 1:1,000 and 1:250, respectively. Cells were washed three times with PBS and further incubated for 30 min with secondary Alexa Fluor 488-conjugated goat anti-mouse or Alexa Fluor 594-conjugated goat-anti rabbit Abs (Invitrogen) at 1:400 dilutions. The samples were mounted with Vectashield mounting medium (Invitrogen) containing DAPI (4′,6-diamidino-2-phenylindole) to visualize the nuclei and analyzed under a Zeiss LSM 710 laser-scanning confocal microscope using a 63× objective. Images were processed with ZEN software.

Flow cytometry analysis. Cells were seeded in six-well plates and maintained for 3 days in the presence or absence of 1 μg/ml Tet. To investigate the internalization of hTfn, cells were starved in serum-free medium for 1 h at 37°C, followed by incubation with 50 μg/ml hTfn-Alexa Fluor 488 for 30 min at 4°C. Unbound hTfn was removed by washing with PBS, and cells were further incubated for 30 min at 37°C in complete medium. Noninternalized ligand was removed by treatment with 0.05% trypsin–EDTA followed by washing with PBS, before the fluorescence-activated cell sorter (FACS) analysis. For LysoTracker internalization, the cells were rapidly detached with 0.05% trypsin–EDTA before incubation with 75 nM LysoTracker Green Dnd-26 (Invitrogen) for 3 min. Duplicate samples from two independent experiments were analyzed using the FACS Calibur and the Cell Quest Pro software.

HBV infection assay. HepaRG cells were differentiated as described in reference 5. A 300-fold-concentrated supernatant of HepG2.2.2.15 cells containing 10^4 HBV genome equivalents (Geq)/cell was used as viral inoculum. Infection was performed in the presence of 4% polyethylene glycol 8000 for 24 h at 37°C as described previously (26). In experiments addressing the effect of Rab proteins silencing on HBV life cycle, 1 μg/ml Tet was added at day 3 prior to viral inoculation and maintained to day 3 postinfection (p.i.); in a different setting, Tet treatment was applied from days 7 to 14 p.i., as indicated in the figure legends. When the effects of different inhibitors were monitored, the cells were incubated with medium containing 400 μM buthionine sulfoximine (BSO), 50 nM bafilomycin A (Baf), 50 mM NH_4Cl or 100 μM E64d. The drugs were added either after removal of the HBV inoculum (BSO) or 24 h later (BSO, Baf, NH_4Cl, and E64d) and were maintained for 24 h. Infected cells were harvested 14 days p.i., and the encapsidated viral DNA was quantified by real-time PCR. All infection experiments were performed with duplicate samples and repeated at least three times.

Quantification of HBV DNA by real-time PCR. HBV-infected HepaRG cells were harvested, and intracellular encapsidated viral DNA was purified by phenol-chloroform extraction, as described elsewhere (27). The DNA was quantified using a Corbett Rotor-Gene 6000 real-time PCR system and Maxima SYBR green quantitative PCR (qPCR) master mix (Fermentas), following amplification of a 279-bp HBV-specific fragment. The number of viral Geq was determined using a calibration curve containing serial dilutions of known amounts of a pTriEx-HBV1.1 vector.

Quantification of HBV replication by Southern blotting. HepG2.2.2.15$^{tetR/shRab5}$ and HepG2.2.2.15$^{tetR/shRab7}$ cells were induced with 1 μg/ml Tet for 3 days or maintained untreated as a control. Treatment with 10 μM lamivudine (3TC; Moravek Biochemicals) was also included as a control of inhibition of viral replication. An equal number of cells were used to extract nucelocapsid viral DNA, following the same procedure as for real-time PCR. The purified DNA was separated on a 1.2% agarose gel and transferred to a Hybond-N membrane (GE Healthcare), using a vacuum transfer blotter (Bio-Rad). The blot was hybridized with a fluorescein-labeled probe obtained by random priming using the HBV DNA genome as the template. Detection of the HBV-specific DNA bands was described previously (27).

Subcellular fractionation of HBV-infected cells. HepaRG cells were differentiated in collagen-coated T75 flasks and infected with 10^4 HBV Geq/cell, for 24 h. Following removal of the viral inoculum, the cells were washed extensively with PBS containing 0.05% trypsin–EDTA to remove any bound and noninternalized virions. The cells were further incubated for either 24 or 48 h, extensively washed with PBS, and harvested with 0.05% trypsin–EDTA. The pellet obtained following centrifugation of cells for 5 min at 2,000 × *g* was washed twice with TS buffer (0.25 M sucrose, 10 mM Tris-Cl [pH 7.4]) then resuspended in 3 ml TS buffer on ice. Samples were homogenized with 40 strokes in a Douncer on ice, followed by centrifugation at 1,000 × *g* for 20 min at 4°C. The supernatant was centrifuged at 6,000 × *g* for 20 min at 4°C. The resulting supernatant was resolved in a 30% Percoll gradient by centrifugation in a 70Ti rotor of the OptimaXPN-100 Beckman ultracentrifuge at 28,000 rpm for 45 min at 4°C. A first fraction of 9 ml was collected from the top, followed by 20 fractions of 0.6 ml. The Percoll was removed following 3-fold dilution of each fraction in TS buffer and centrifugation at 25,000 × *g* for 45 min at 4°C. The pellets were split in two and used to quantify the amount encapsidated viral DNA by real-time PCR or to determine the distribution of intracellular markers by SDS-PAGE and Western blotting using anti-Lamp1 (dilution, 1:200), anti-Crt, and anti-cathepsin D (dilution 1:2,000) Abs (Abcam).

RESULTS

Characterization of HepaRG cell lines with tetracycline-inducible, downregulated Rab5, Rab7, Rab9, or Rab11 expression. Interference with expression of key regulators of the endocytic pathway is widely used to investigate viral entry, the Rab proteins being very good candidates for such a task (28–31). However, genetic manipulation is very problematic for primary hepatic or differentiated HepaRG cells, mainly because of the very low transfection efficiency. Therefore, to investigate the trafficking events following HBV endocytosis, newly HepaRG cell lines were established, stably and controllably expression of shRNA molecules targeting Rab5, Rab7, Rab9, and Rab11. This inducible gene expression system brings an enormous advantage over other approaches, by eliminating the discrepancies due to clonal variation and has been successfully applied for HepaRG to investigate the role of the HBx protein in HBV replication (32).

The new HepaRG clones were analyzed for the expression of the corresponding Rab proteins, in the absence and presence of the inducer, by Western blotting using specific Abs. As shown in Fig. 1, addition of Tet to the cell medium resulted in a significant reduction of Rab5 biosynthesis in HepaRG$^{tetR/shRab5}$ cells but not in the cell lines bearing shRNA targeted to either Rab7, Rab9, or Rab11 (Fig. 1A). Similarly, Rab7 expression was downregulated in HepaRG$^{tetR/shRab7}$ cells; however, it was unaffected in the remaining cell lines (Fig. 1B). The same behavior was observed for Rab9 and Rab11 when their expression was analyzed in all four HepaRG

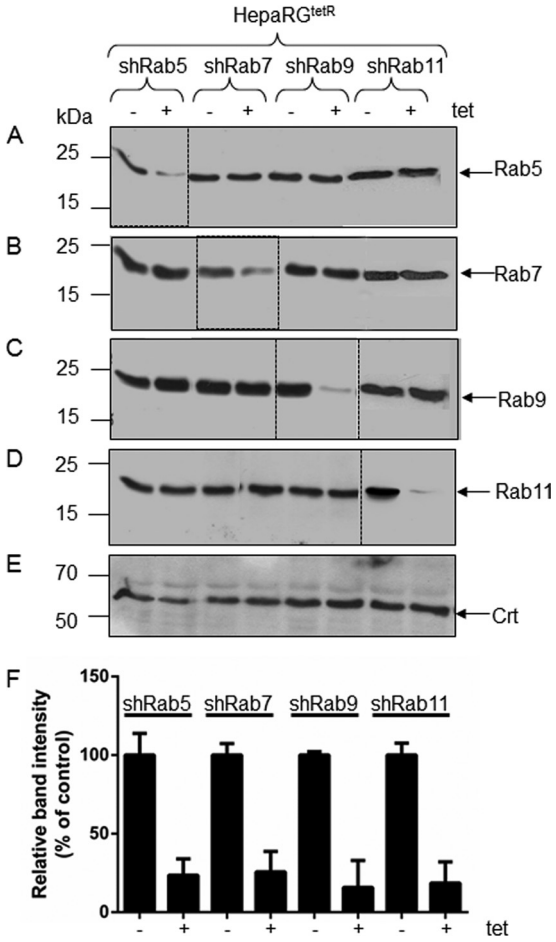

FIG 1 Biosynthesis of Rab proteins in HepaRG$^{tetR/shRab5}$, HepaRG$^{tetR/shRab7}$, HepaRG$^{tetR/shRab9}$, and HepaRG$^{tetR/shRab11}$ cells. HepaRG cells stably expressing shRNA specific for the indicated Rab proteins were either induced with 1 μg/ml Tet for 3 days (+) or maintained untreated (−) as a control. The total protein content in cell lysates was quantified, and equal amounts were loaded for SDS–10% PAGE. Depletion of the Rab proteins was confirmed by Western blotting using anti-Rab5 (A), anti-Rab7 (B), anti-Rab9 (C), and anti-Rab11 (D) Abs. Crt levels in the same cell lysates were detected with specific Abs and used as a loading control (E). The representative blots from three independent experiments are shown. Quantification of the blotted proteins was performed using the Quantity One software. The error bars represent the standard deviations (SD) among three independent experiments (F).

clones (Fig. 1C and D). The level of Crt, a soluble endoplasmic reticulum (ER)-resident protein was also measured as a control (Fig. 1E). Downregulation of Rab protein synthesis in the presence of inducer was quantified using the Quantity One software (Fig. 1F). Together, the results suggest that Tet induction was efficient at silencing the expression of each of the Rab proteins considered in this experiment and, importantly, downregulation of a specific Rab did not impact the expression of the other Rabs in the same cell line.

Functional properties of the HepaRG$^{tetR/shRab5}$, HepaRG$^{tetR/shRab7}$, HepaRG$^{tetR/shRab9}$, and HepaRG$^{tetR/shRab11}$ cell lines. Very recently, an unexpected resilience of the endocytic pathway to perturbations in the concentration of key regulator molecules was documented *in vivo* (33). Therefore, to determine the consequences of the Rab proteins' silencing on the trafficking properties of the newly developed HepaRG cells, the subcellular distribution of a series of well-established markers of intracellular pathways was next investigated.

The iron-loaded protein Tfn is internalized through its receptor (TfnR) and delivered to the early/sorting endosome in a Rab5-dependent process (34). Most of the internalized TfnR is trafficked back to the plasma membrane through the recycling endosomes regulated by Rab11 (23, 35). Endocytosis of fluorescently labeled hTfn and confocal microscopy were used to determine the effect of Rab5 and Rab11 depletion on the endocytic properties of the new HepaRG cell lines. As shown in Fig. 2A and B, hTfn was readily internalized in noninduced HepaRG$^{tetR/shRab5}$ and HepaRG$^{tetR/shRab11}$ cells. Dual immunolabeling showed a partial colocalization with both Rab5 in vesicular compartments distributed more centrally within the cytoplasm, as previously shown for early endosomes (36) (Fig. 2A), and Rab11 in structures more diffusely distributed throughout the cell, partially enriched in the perinuclear area, characteristic of recycling endosomes (Fig. 2B) (37). Following Tet induction, the amount of internalized hTfn decreased significantly in HepaRG$^{tetR/shRab5}$ cells, with a fraction of the fluorescent marker accumulating in the vicinity of the plasma membrane (Fig. 2A, arrow). A similar behavior was observed for HepaRG$^{tetR/shRab11}$ cells, where prevention of the TfnR recycling to the plasma membrane resulted in less fluorescent ligand being endocytosed (Fig. 2B). Consistent with the results obtained by Western blotting, a strong depletion of Rab5 and Rab11 was readily observed in the corresponding Tet-induced HepaRG cells (Fig. 2A and B).

These observations were further confirmed following quantitative measurement of the internalized fluorescence by FACS analysis (Fig. 2C).

To investigate the impact of Rab7 downregulation on the organization of the endolysosomal compartment, we monitored the distribution of the lysosomal-associated membrane protein 1 (Lamp1), a major lysosomal membrane protein (38), in HepaRG$^{tetR/shRab7}$ cells, in the presence or absence of the inducer. Dual labeling using Lamp1- and Rab7-specific Abs followed by confocal microscopy analysis revealed three distinct populations of vesicles in untreated cells, Rab7 or LAMP1 positive or containing both markers, and these populations were more concentrated around the nucleus (Fig. 3A), which is consistent with the results shown previously in intact live cells (39). In contrast, the loss of Rab7 expression in Tet-induced cells was accompanied by Lamp1 dispersion from the juxtanuclear region, in smaller vesicles scattered throughout the cytosol. A similarly altered intracellular distribution was observed following expression of Rab7 dominant-negative variants in HeLa cells, which resulted in functionally defective lysosomes. Moreover, acidification of the dispersed lysosomes was significantly perturbed in these cells in the absence of a continuous supply of vacuolar proton ATPase from the *trans*-Golgi network (21).

The changes of the endolysosomal compartment properties in HepaRG$^{tetR/shRab7}$ cells were also quantified by FACS using LysoTracker, a membrane-permeable probe accumulating in acidic organelles (40). As shown in Fig. 3B, the intensity of the fluorescent signal was reduced by 70% in induced cells compared to controls, demonstrating that Rab7 silencing was achieved at a sufficient level to impact the lysosomal function.

Mannose 6-phosphate receptors (MPRs) carry lysosomal en-

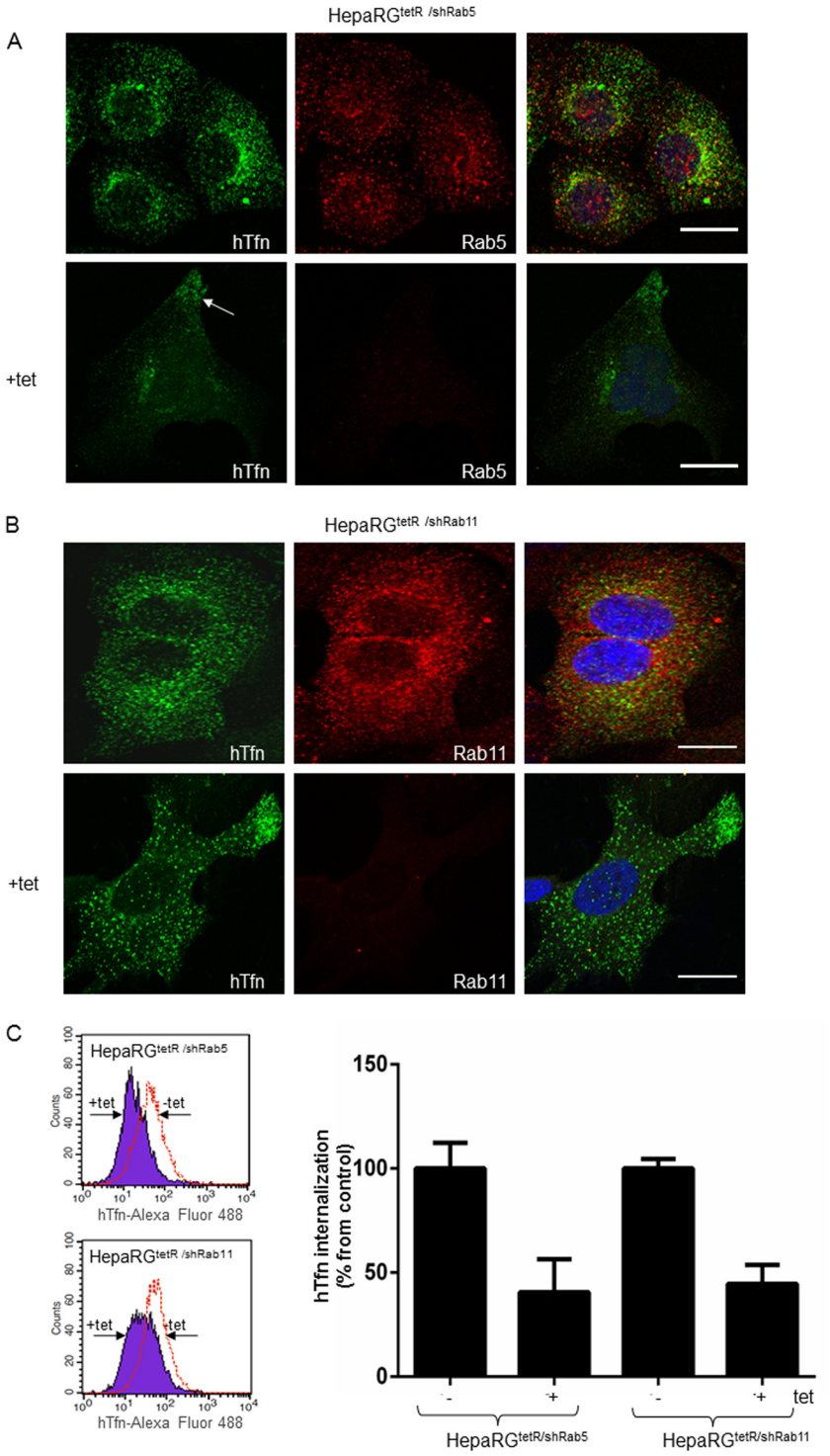

FIG 2 Functional characterization of the HepaRG$^{tetR/shRab5}$ and HepaRG$^{tetR/shRab11}$ cells. Cells were incubated with 1 μg/ml Tet or maintained untreated. After 3 days, 50 μg/ml hTfn-Alexa Fluor 488 was added for 30 min at 4°C, and then cells were moved to 37°C for 30 min. Intracellular distribution of Rab5 (A) and Rab11 (B) was evidenced using specific Abs and the Zeiss LSM 710 confocal microscope following mounting with Vectashield mounting medium containing DAPI, to visualize the nuclei (blue). Images were taken with the 63× objective and processed with ZEN software. Scale bar is 20 μm. Internalization of hTfn-Alexa Fluor 488 was investigated by flow cytometry using the FACS Calibur and the Cell Quest Pro software. Representative histograms from two independent experiments run with duplicate samples are shown. The values are the geometric mean (±SD) fluorescence of Tet-treated samples represented as percentage from control (C).

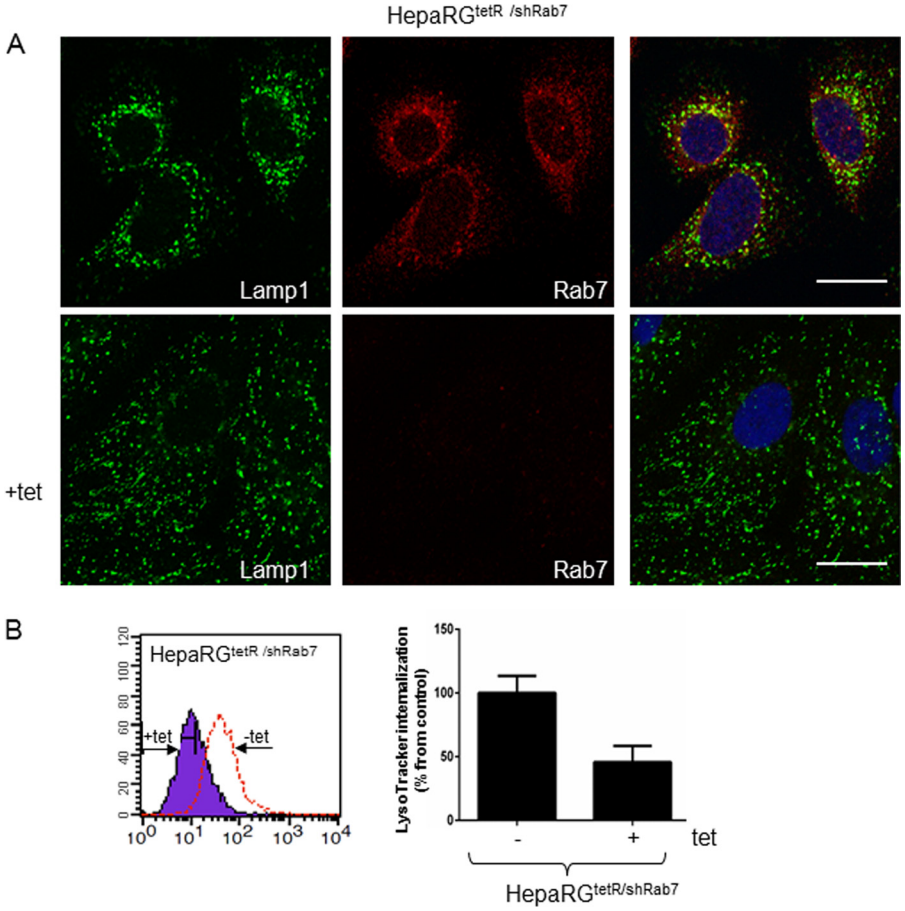

FIG 3 Functional characterization of the HepaRG$^{tetR/shRab7}$ cells. Cells were either induced with 1 μg/ml Tet or left untreated as a control. The Lamp1 and Rab7 intracellular distribution was demonstrated using specific Abs and the Zeiss LSM 710 confocal microscope following mounting with Vectashield mounting medium containing DAPI to visualize the nuclei (blue). Images were taken with the 63× objective and processed with ZEN software. The scale bar is 20 μm (A). Internalization of LysoTracker Green Dnd-26 was investigated by flow cytometry using the FACS Calibur and the Cell Quest Pro software. Representative histograms from two independent experiments run in duplicate samples are shown. The values are the geometric mean fluorescence of Tet-treated samples represented as a percentage (±SD) of the control (B).

zymes from the *trans*-Golgi network to endosomes and then return to the *trans*-Golgi network in a process regulated by Rab9 (22). As a consequence, MPRs predominantly colocalize with this compartment, while a fraction is also present in Rab9-positive late endosomes (41). We next monitored the intracellular distribution of the cation-independent (CI)-MPRs by confocal microscopy, to characterize the Rab9-dependent trafficking in the HepaRG$^{tetR/shRab9}$ cells. As expected, in cells expressing normal levels of Rab9, CI-MPRs were concentrated in the perinuclear area, while little staining was observed in punctate vesicles throughout the cytoplasm (42) (Fig. 4A). However, in the absence of Rab9 expression, the latter fraction was more prominent and extended to the cell periphery, consistent with CI-MPR retention within late endosmes and acceleration of the endosome-to plasma membrane transport, described previously (43) (Fig. 4A). Moreover, the LAMP1 staining was reduced in peripheral structures, while a much tighter juxtanuclear localization became dominant, another effect described following Rab9 depletion (43) (Fig. 4B).

Additional control experiments were performed to monitor the distribution of CI-MPRs in Rab5-, Rab7-, and Rab11-depleted cells, as well as that of Lamp1 in the absence of Rab5 or Rab11 expression. The consequences of Rab7 and Rab9 or Rab5 and Rab11 depletion on internalization of hTfn and Lysotracker, respectively, were also investigated. Overall, no significant alteration of the distribution of these markers was observed in cells depleted of the corresponding Rabs, confirming the functional specificity of each Rab silencing (data not shown).

Collectively, the data show that the Rab proteins were specifically and efficiently downregulated in the newly developed HepaRG cell lines, providing reliable tools to investigate the early steps of the HBV life cycle.

HBV infection is dependent on Rab5 and Rab7, but not Rab9 and Rab11 expression. Having established the trafficking properties of the HepaRG$^{tetR/shRab5}$, HepaRG$^{tetR/shRab7}$, HepaRG$^{tetR/shRab9}$, and HepaRG$^{tetR/shRab11}$ cell lines, we next investigated the ability of HBV to initiate productive infection in these cells. All cell lines were differentiated in collagen-coated six-well plates and then either treated with Tet for 3 days or maintained untreated as a control. Cells were further inoculated with equal amounts of virus stock, purified from HepG2.2.2.15 cell supernatants as described above. Induction was discontinued at day 3 p.i., following Tet removal, allowing the silenced Rabs to

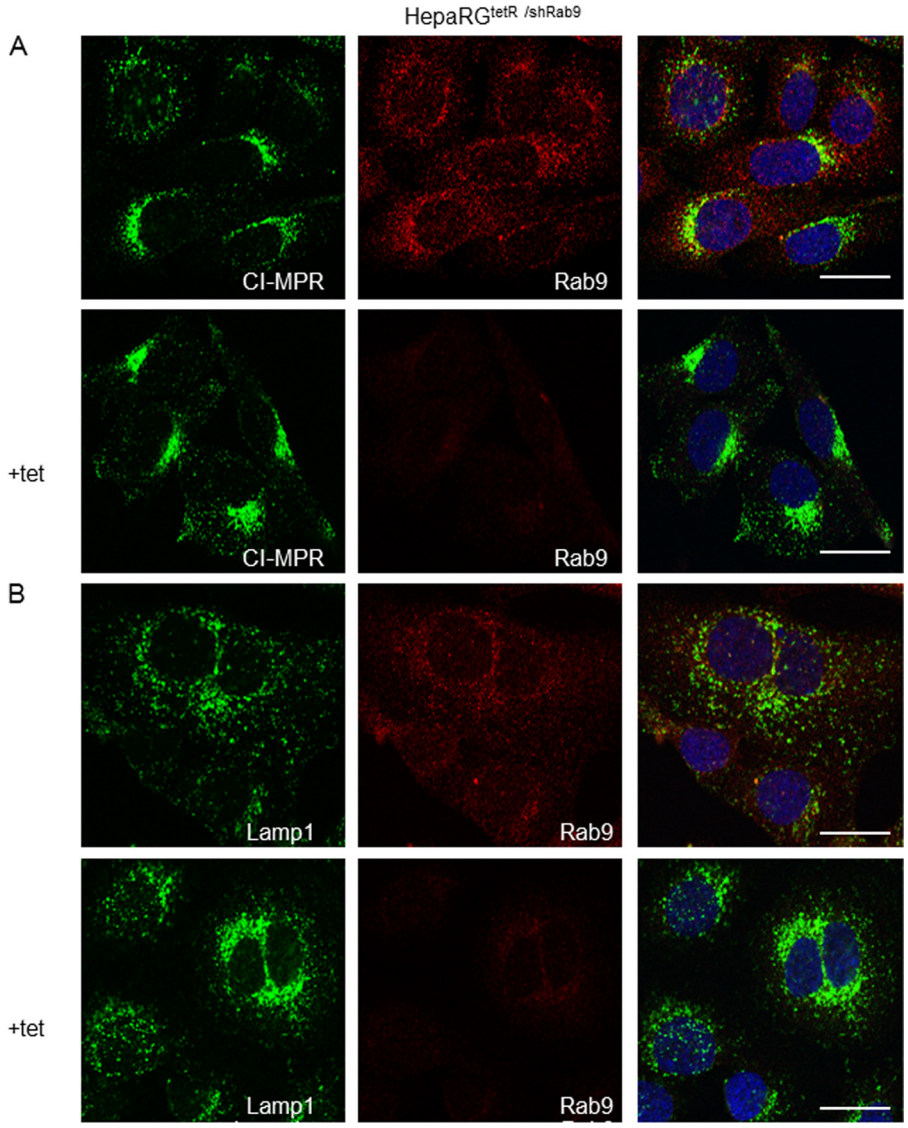

FIG 4 Functional characterization of the HepaRG$^{tetR/shRab9}$ cells. Cells were either induced with 1 μg/ml Tet or left untreated as a control and prepared for immunofluorescence. The intracellular distribution of CI-MPRs (A), Lamp1 (B), and Rab9 (A and B) was demonstrated by using specific Abs and the Zeiss LSM 710 confocal microscope, following mounting with Vectashield mounting medium containing DAPI to visualize the nuclei (blue). Images were taken with the 63× objective and processed with ZEN software. The scale bar is 20 μm.

return to normal levels during viral replication. HBV nucleocapsids were purified from infected cells at day 14 p.i., and the viral DNA was quantified by real-time PCR. As shown in Fig. 5A, a strong inhibition of HBV infection was observed upon induction in both HepaRG$^{tetR/shRab5}$ and HepaRG$^{tetR/shRab7}$ cells, of about 70 and 75%, respectively. In contrast, Rab9 or Rab11 silencing did not have any significant impact on HBV infection (Fig. 5B). These results suggest that the HBV particles enter the endocytic pathway of the host cell and require trafficking as far as late endosomes/lysosomes to initiate an infectious cycle. Moreover, neither the recycling compartment nor the endosomal transport to the *trans*-Golgi network is important in this process.

It was reported that expression of certain shRNA sequences can trigger an interferon response in host cells (44). Since such a potential nonspecific stress response may have antiviral effects on its own, the transcripts of two genes, the *OAS2* and *MX1*, involved in interferon-stimulated pathways, were investigated by reverse transcription-PCR. Neither of the transcripts was found to be upregulated in any of the newly developed HepaRG cell lines (data not shown).

HBV replication is not affected by Rab5 or Rab7 downregulation. To investigate the early steps of viral infection, Rab silencing was performed in a controlled manner, within the first 3 days p.i., when viral replication is at a minimum level in HepaRG cells (5). However, as the outcome of infection is measured at day 14 p.i., a potential direct influence of Rab5 or Rab7 depletion on HBV replication, although unlikely, cannot be completely excluded. To address this possibility, two control experiments were performed. In the first approach, HBV-infected HepaRG$^{tetR/shRab5}$ and HepaRG$^{tetR/shRab7}$ cells were treated with Tet during viral replication, between days 7 and 14 p.i., and the amount of nucleocapsids was quantified by real-time PCR, as

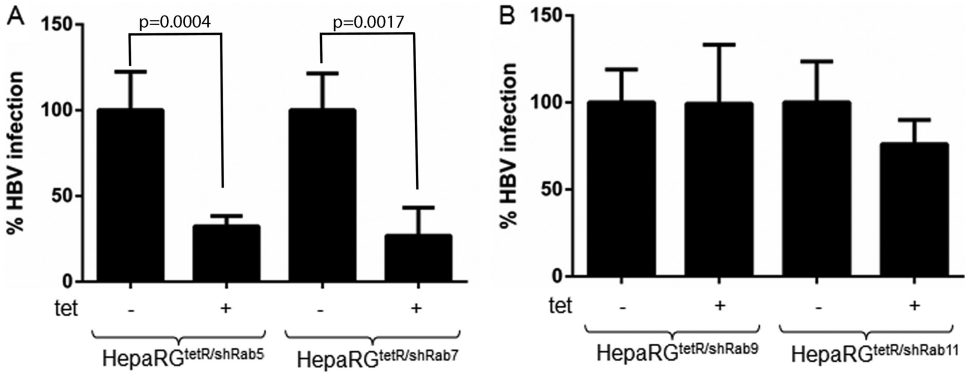

FIG 5 HBV infection in Rab-depleted cells. Differentiated cells were treated with 1 μg/ml Tet for 3 days (+) or maintained untreated (−) before infection with 10^4 HBV Geq/cell. Treatment was discontinued at day 3 p.i. Infected cells were harvested 14 days p.i., and the amount of encapsidated viral DNA was quantified by real-time PCR. The results are expressed as the percentage of HBV infection from untreated controls. The error bars represent the SD between three independent experiments, each run in duplicate samples (A and B).

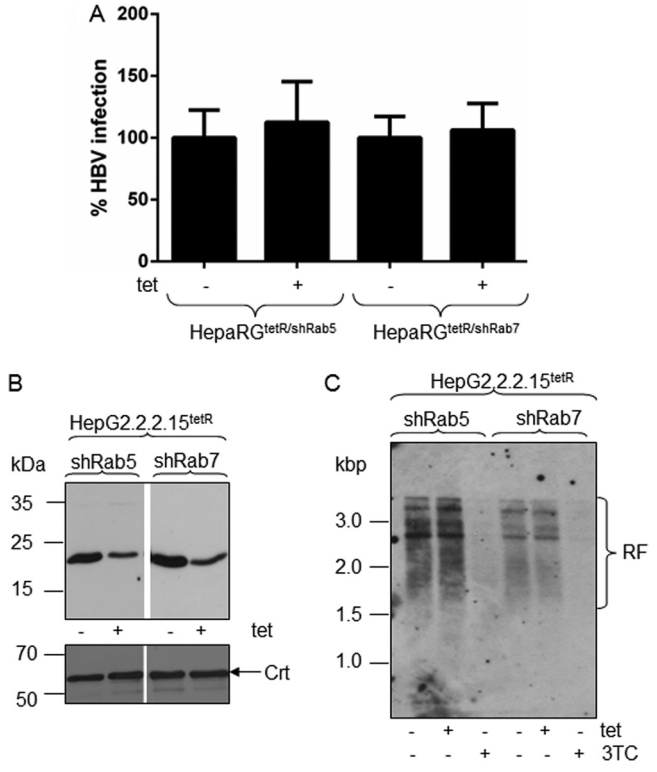

FIG 6 HBV replication in Rab-depleted cells. Differentiated HepaRG$^{tetR/shRab5}$ and HepaRG$^{tetR/shRab7}$ cells were infected with 10^4 HBV Geq/cell and then treated with 1 μg/ml Tet from day 7 to day 14 p.i. (+) or maintained untreated (−) as the control. Infected cells were harvested 14 days p.i., and the amount of encapsidated viral DNA was quantified by real-time PCR. The results are expressed as percentage of HBV infection from untreated controls. The error bars represent the standard deviations among three independent experiments, each run in duplicate samples (A). HepaG2.2.2.15$^{tetR/shRab5}$ and HepaG2.2.2.15$^{tetR/shRab7}$ cells were induced with 1 μg/ml Tet for 3 days or maintained untreated as a control. Depletion of Rab5 and Rab7 was confirmed by Western blotting using specific Abs and Crt expression as a loading control (B). HepG2.2.2.15$^{tetR/shRab5}$ and HepG2.2.2.15$^{tetR/shRab7}$ cells were treated with 1 μg/ml Tet or 10 μM 3TC for 3 days or maintained untreated as a control. HBV nucleocapsids were extracted from an equal number of cells, and the purified DNA was analyzed by Southern blotting. The HBV replication forms (RF) were detected with a fluorescein-labeled probe obtained by random priming using the HBV DNA genome as the template (C).

above. As shown in Fig. 6A, neither Rab5, nor Rab7 silencing had any significant effect on the viral DNA level. In a second approach, Rab5 and Rab7 depletion was achieved in HepG2.2.2.15 cells, which are not permissive for HBV infection, using the same Tet-controlled shRNA expression system employed for the HepaRG cells. The decreased amount of Rab5 and Rab7 proteins in induced cells was confirmed by Western blotting (Fig. 6B). Southern blotting was further used to monitor the HBV replication in the newly established HepaG2.2.2.15$^{tetR/shRab5}$ and HepaG2.2.2.15$^{tetR/shRab7}$ cells, in the presence or absence of inducer. Lamivudine (3TC), a potent HBV replication inhibitor was also included in the experiment as a control. As shown in Fig. 6C, Tet treatment had no impact on the HBV replication forms (RF) in either HepG2.2.2.15 cell line, while 3TC inhibited replication almost completely, as expected.

Together, the results demonstrate that the inhibitory effects of Rab5 and Rab7 described in the section above clearly address the early stages of viral entry.

HBV is trafficked to the degradative branch of the endocytic pathway. To further characterize the compartments traversed by HBV following internalization, a subcellular fractionation experiment was performed with HepaRG cells at 24 and 48 h p.i. by ultracentrifugation in a 30% Percoll gradient. This type of gradient has been used before to separate endocytic vesicles in two distinct populations: a light fraction consisting of early endosomes and heterogeneous secretory vesicles and a heavier fraction mainly composed of late endosomes/lysosomes (45).

The postnuclear fractions were collected from top to bottom and characterized for the presence of different endocytic markers by Western blotting and viral nucleocapsids by real-time PCR. Lamp1 was concentrated in fractions 2 to 6, which were also positive for the ER-resident protein Crt, and fractions 15 to 20, which were heavily loaded with the 34-kDa, mature cathepsin D chain characteristic of the lysosomal compartment (46) (Fig. 7A). These results are consistent with Lamp1 being shuttled between lysosomes and endosomes and confirm the successful separation of the endolysosome heavy fraction from the remaining heterogenous vesicles. Interestingly, purification of the HBV particles from the collected fractions showed that the virus is distributed along the endocytic pathway during 24 h p.i., mainly in the light endosomal vesicles. In contrast, the major pool of HBV particles is

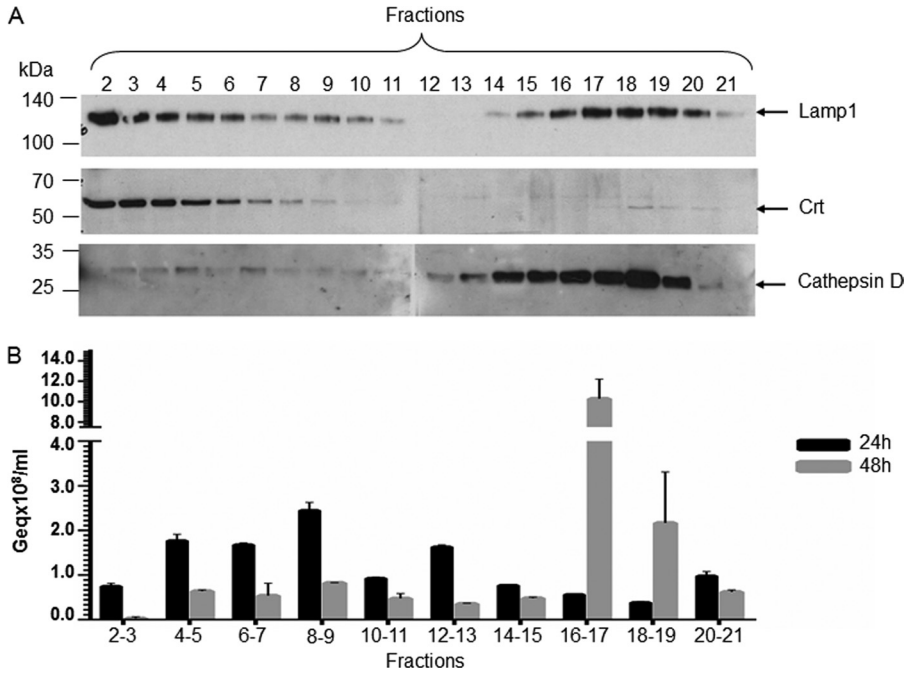

FIG 7 HBV distribution in HepaRG cells at early stages of infection. Differentiated HepaRG cells were infected with10^4 HBV Geq/cell for 24 h. The viral inoculum was removed by extensive washing with PBS-EDTA, and the cells were harvested after incubation for either 24 or 48 h. Samples were homogenized in a Douncer and resolved in a 30% Percoll gradient by ultracentrifugation. Fractions were collected from the top of the gradient and analyzed for the distribution of intracellular markers by SDS-PAGE and Western blotting (A) or the presence of HBV particles following DNA purification and quantitative real-time PCR (B). The representative blots from two independent experiments are shown (A). The error bars represent the SD between two independent experiments run with triplicate samples (B).

concentrated in nucleocapsids in Lamp1 and cathepsin D-labeled endolysosomes at 48 h p.i., an indicator of the transport to the degradative branch (Fig. 7B). To determine the nature of the HBV particles reaching this location, the endolysosomal fractions were pooled and subjected to immunoprecipitation with either anti-capsid or anti-S Abs followed by purification of the viral DNA and quantification by real-time PCR. Comparable amounts of viral DNA were isolated in both immunoprecipitates, suggesting that this fraction contains enveloped as well as naked particles (data not shown).

It was previously demonstrated that pharmacological agents known to elevate the pH of endosomes and lysosomes have no impact on HBV or DHBV infections when cells are pretreated with these reagents (12, 47). To determine whether the inhibition of lysosomal function has any impact on HBV infectivity, we have retested Baf and NH_4Cl by adding the drugs at 24 h p.i. and maintaining the treatment for another 24 h. The protease inhibitor E64d was also included in this experiment. Despite the longer treatment applied, these inhibitors remained without effect (Fig. 8A), suggesting that the lysosomal proteolytic activity does not play an active role in infection; rather, the virus may be transported to this compartment to be further degraded and thus removed from the endocytic system.

In addition to providing an acidic environment and various proteolytic enzymes, the late endosomes also ensure a reducing milieu which favors processing of disulfide-linked envelope

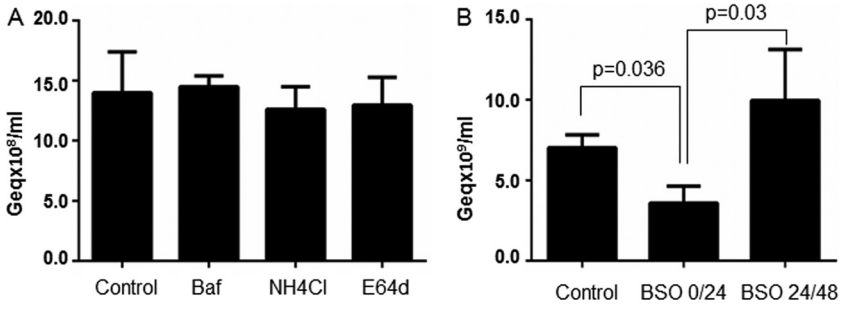

FIG 8 HBV infection in the presence of inhibitors of endocytic pathways redox potential and proteolytic activity. Differentiated cells were infected with 10^4 HBV Geq/cell and then incubated with medium containing 50 nM Baf, 50 mM NH_4Cl, 100 μM E64d (A) or 400 μM BSO (B). The drugs were added either after removal of the HBV inoculum (BSO) or 24 h later (BSO, Baf, NH_4Cl, and E64d) and were maintained for 24 h. Infected cells were harvested 14 days p.i. and the encapsidated viral DNA was quantified by real-time PCR. The results are expressed as percentages of HBV infection from untreated (no drug) controls. The error bars represent the SD among three independent experiments, each run with duplicate samples (A and B).

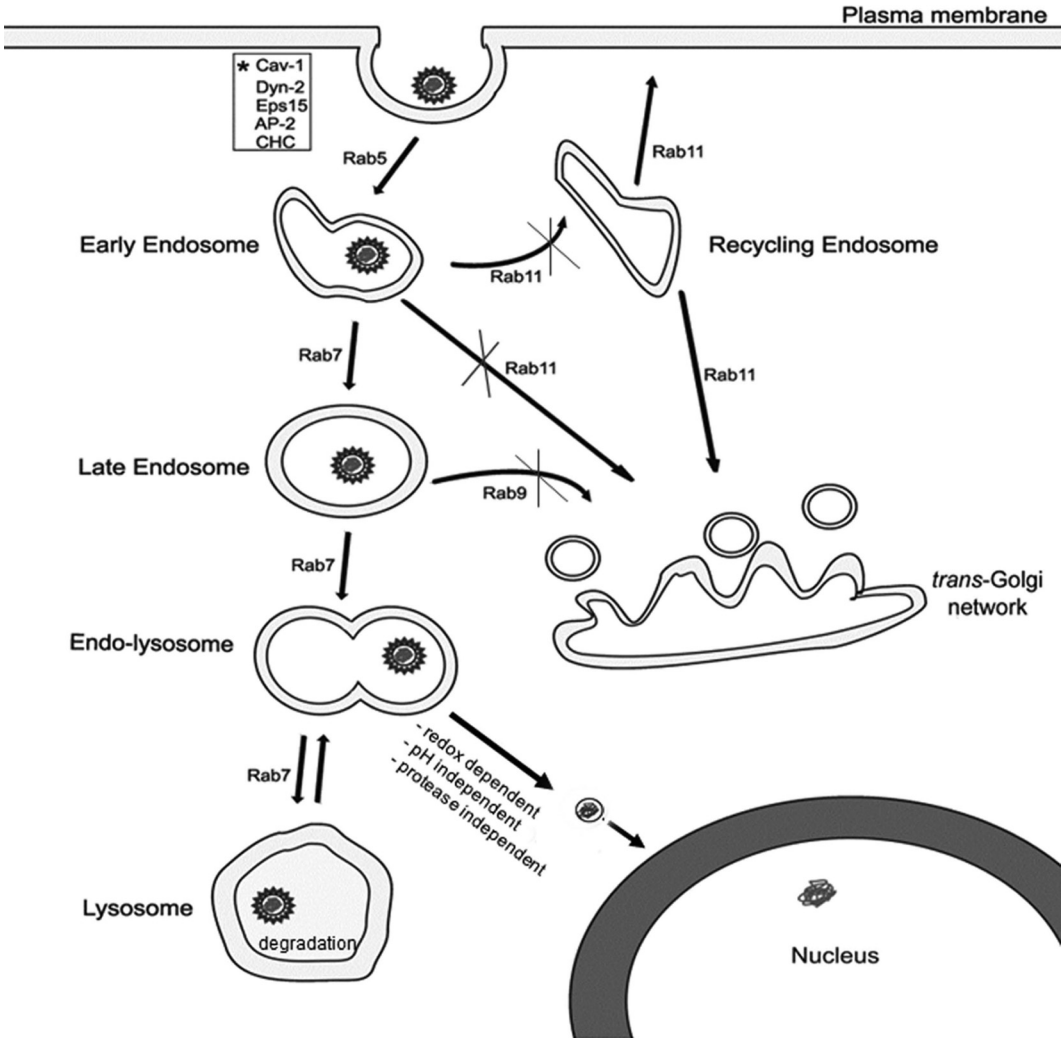

FIG 9 Schematic representation of HBV trafficking following internalization in HepaRG cells. HBV infection depends on Rab5 and Rab7 transport through the endocytic pathway, while neither the recycling endosomes nor the vesicles en route to the *trans*-Golgi network play a role in this process. Viral uncoating occurs in a compartment preceding the lysosomes, in a redox-potential-dependent, pH- and proteolytic activity-independent manner. Further transport to lysosomes has no influence on infection, indicating a role in viral disposal. Other proteins shown to play a function in HBV infection are marked with an asterisk.

proteins and could potentially facilitate virus release from the endocytic compartment (48). To test if this hypothesis applies to HBV, we depleted the cells of glutathione (GSH), by using BSO, a membrane-permeable inhibitor that irreversibly inhibits γ-glutamylcysteine synthetase, the enzyme required for GSH biosynthesis (49). Interestingly, BSO treatment within the first 24 h p.i. resulted in about 55% reduction of HBV infection, while the inhibitory effect was abolished when the drug was added at later points p.i. (Fig. 8B). This suggests that a reduction step along the endocytic pathway is required for initiation of a productive infection.

DISCUSSION

Although important advances have been made in recent years toward understanding HBV entry into host cells, many issues remain unclear. Very recently, NTCP, a liver bile acid transporter, was proposed as a potential receptor for HBV (13). NTCP overexpression in cell lines that are not permissive for HBV infection rendered them susceptible; however, the efficiency of the infection remained intriguingly low, despite these cells being able to ensure high levels of virus replication when the entry steps are bypassed by transfection of the viral genome. This strongly suggests that plasma membrane receptors are not the only limiting factors of infection, other yet unidentified cellular factors may significantly contribute to this process at its very early steps.

This study addressed the unexplored HBV fate, postinternalization in HepaRG cells. By depleting the cells of several key Rab proteins in a controlled manner, we were able to monitor the intracellular trafficking of HBV particles following endocytosis. The data show that HBV requires Rab5- and Rab7-dependent transport through the endosomal compartment to initiate a successful infection, while neither the recycling endosomes nor the vesicles en route to *trans*-Golgi network are involved in this process (summarized in Fig. 9). The use of early endocytic pathway by the HBV particles is not in disagreement with our previous results reporting a dependence on functional caveolin-1 for productive

infection (12). Recent studies have linked caveolin to conventional endocytic trafficking pathways and the existence of the caveosome, the unique transport organelle involved in caveola-mediated endocytosis, is now doubted (50).

The results of this study imply that viral particles enter early endosomes that progress to late endosomes where the appropriate environment may provide the signal for the release of the viral genome into the cytoplasm, leading to infection. Trafficking through endosomes is known to be important for viruses that depend on low pH or endosomal proteases to facilitate uncoating (51, 52). However, acidification does not appear to be an essential factor for HBV infection, as extended cell treatment with Baf or NH_4Cl did not affect this process; similarly, inhibition of endosomal cathepsin activity remained without having any consequences on the infection outcome. This intriguing behavior is not singular to HBV; other viruses, such as echovirus 7, use the endocytic trafficking to initiate infection in a pH- and protease activity-independent manner (53). One possible interpretation is that trafficking through endosomes, albeit essential, may only represent an intermediate step leading to a cellular organelle where the viral genome is released. For instance, it has been shown that canine parvovirus and mouse polyomavirus use the recycling endosomes to finally reach the lysosomes and the ER, respectively (54, 55); however, the recycle compartment was clearly shown to be dispensable for HBV infection. Alternatively, the late endosomes may host another factor essential for HBV uncoating. The structure of the HBV envelope is stabilized by extensive intra- and intermolecular disulfide cross-linking of the component polypeptides (56), thus the disulfide bond-reducing activity of the endocytic pathway is a good candidate for such a function (57, 58). Using fluorescence resonance energy transfer (FRET)-based imaging, it was shown that the disulfide reduction machinery is activated upon internalization of a folate-FRET reporter into endosomes, independent of the interaction of this compartment with the lysosomes or the Golgi apparatus (59). Such activity requires deprotonation of thiols, which is not favored thermodynamically by the acidic environment of the endosome, suggesting that most likely, an enzymatic catalysis is involved (59). Interestingly, entry of other enveloped viruses, such as the human immunodeficiency virus (HIV), depends on a reduction step involving a cell-surface protein disulfide isomerase (PDI)-related protein (60, 61). However, this does not appear to be the case for HBV, since treatment of cells with either membrane-impermeable compounds that alter the redox state of surface-exposed cysteine residues or PDI inhibitors had no effect on infection (62). In our study, the kinetics of HBV infection in the presence of the membrane-permeable GSH biosynthesis inhibitor favors the hypothesis of thiol-disulfide exchange occurring in an internal cellular compartment, not at the cell surface. Indeed, BSO efficiently inhibited HBV early in infection but not at later points, implying that the reduction step is restricted to a particular location along the endocytic pathway. We are currently employing extensive proteomic analysis to identify additional host factors associated with the redox machinery of the endocytic pathway with a potential role in infection, using an approach described before for the plasma membrane proteins (63).

Monitoring of viral entry by single-particle tracking has not been possible for HBV, as infection efficiency is very low *in vitro* and attempts to label functional HBV virions have failed so far, despite successful approaches being described for SVP (64, 65). As an alternative, here we have employed subcellular fractionation and amplification of encapsidated viral DNA to further examine the intracellular distribution of internalized virions. After uptake by differentiated HepaRG cells, the viral particles were found dispersed into a fraction of heterogeneous endocytic vesicles, consisting of early and late endosomes, while they later were concentrated into lysosomes, suggesting that viral nucleocapsids remain intact in the endocytic pathway for at least several days. This is consistent with the observation made during the first characterization of the HepaRG cell line, showing that the input viral particle level is relatively stable, being detected within the cells for at least 2 days (5). Moreover, enveloped virus particles were immunoprecipitated in the lysosomal fraction, which is an indication that uncoating in a previous compartment is a rather inefficient process, in competition with trafficking further down the degradation pathway. The HBV transport to lysosomes remains intriguing, as no evidence for a role of this compartment in promoting infection could be demonstrated. Interestingly, it has been shown that a fraction of HIV particles bound to target cells is taken up by endocytosis but remains entrapped in the endocytic pathway and fails to initiate infection, eventually being targeted to lysosomes for degradation (66). Following cell treatment with pharmacological agents that increase the pH of endosomes and lysosomes, HIV-1 infection was greatly enhanced suggesting that the virus is able to escape from lysosomes when rescued from degradation (66). This behavior was not observed for HBV; rather, the trafficking into the endocytic degradative branch appears to be a dead-end pathway, possibly as a part of the cell defense mechanisms to limit the number of viral particles available to initiate productive infection. This hypothesis is supported by the observation that internalized HBV core particles are transported to lysosomes and further disassembled as a result of endoproteolytic cleavage within the arginine-rich domain of the core polypeptide, by cysteine proteases (67).

Taken together, these studies indicate that HBV transport through early and late endosomal compartments is a viable pathway leading to productive infection in HepaRG cells. Future experiments should establish whether the lysosomal trafficking and accumulation of the viral particles in this compartment are contributing factors to the unusual low efficiency of HBV infection *in vitro*, characterized by low kinetics and requiring a high concentration of virus inoculum (26).

ACKNOWLEDGMENTS

This work was supported by the Romanian Academy Project 3 of the Institute of Biochemistry. Alina Macovei and Catalin Lazar were supported by the Sectoral Operational Programme Human Resources Development POSDRU/89/1.5/S/60746 grant. Catalina Petrareanu was supported by the Sectoral Operational Programme Human Resources Development 2007–2013 of the Romanian Ministry of Labor, Family and Social Protection through Financial Agreement POSDRU/107/1.5/S/76903.

REFERENCES

1. **Ganem D, Prince AM.** 2004. Hepatitis B virus infection—natural history and clinical consequences. N. Engl. J. Med. **350**:1118–1129.
2. **Bruss V.** 2007. Hepatitis B virus morphogenesis. World J. Gastroenterol. **13**:65–73.
3. **Zuckerman AJ.** 1996. Hepatitis viruses. Chapter 70. *In* Baron S (ed), Medical microbiology, 4th ed. University of Texas Medical Branch, Galveston, TX.
4. **Heermann KH, Goldmann U, Schwartz W, Seyffarth T, Baumgarten H, Gerlich WH.** 1984. Large surface proteins of hepatitis B virus containing the pre-*s* sequence. J. Virol. **52**:396–402.

5. **Gripon P, Rumin S, Urban S, Le Seyec J, Glaise D, Cannie I, Guyomard C, Lucas J, Trepo C, Guguen-Guillouzo C.** 2002. Infection of a human hepatoma cell line by hepatitis B virus. Proc. Natl. Acad. Sci. U. S. A. **99**:15655–15660.
6. **Huang HC, Chen CC, Chang WC, Tao MH, Huang C.** 2012. Entry of hepatitis B virus into immortalized human primary hepatocytes by clathrin-dependent endocytosis. J. Virol. **86**:9443–9453.
7. **Aly HH, Watashi K, Hijikata M, Kaneko H, Takada Y, Egawa H, Uemoto S, Shimotohno K.** 2007. Serum-derived hepatitis C virus infectivity in interferon regulatory factor-7-suppressed human primary hepatocytes. J. Hepatol. **46**:26–36.
8. **Paganelli M, Dallmeier K, Nyabi O, Scheers I, Kabamba B, Neyts J, Goubau P, Najimi M, Sokal EM.** 2013. Differentiated umbilical cord matrix stem cells as a new in vitro model to study early events during hepatitis B virus infection. Hepatology **57**:59–69.
9. **Schulze A, Gripon P, Urban S.** 2007. Hepatitis B virus infection initiates with a large surface protein-dependent binding to heparan sulfate proteoglycans. Hepatology **46**:1759–1768.
10. **Leistner CM, Gruen-Bernhard S, Glebe D.** 2008. Role of glycosaminoglycans for binding and infection of hepatitis B virus. Cell. Microbiol. **10**:122–133.
11. **Sureau C, Salisse J.** 2013. A conformational heparan sulfate-binding site essential to infectivity overlaps with the conserved hepatitis B virus A-determinant. Hepatology **57**:985–994.
12. **Macovei A, Radulescu C, Lazar C, Petrescu S, Durantel D, Dwek RA, Zitzmann N, Nichita NB.** 2010. Hepatitis B virus requires intact caveolin-1 function for productive infection in HepaRG cells. J. Virol. **84**:243–253.
13. **Yan H, Zhong G, Xu G, He W, Jing Z, Gao Z, Huang Y, Qi Y, Peng B, Wang H, Fu L, Song M, Chen P, Gao W, Ren B, Sun Y, Cai T, Feng X, Sui J, Li W.** 2012. Sodium taurocholate cotransporting polypeptide is a functional receptor for human hepatitis B and D virus. eLife **1**:e00049. doi:10.7554/eLife.00049.
14. **Martinez O, Goud B.** 1998. Rab proteins. Biochim. Biophys. Acta **1404**: 101–112.
15. **Zerial M, McBride H.** 2001. Rab proteins as membrane organizers. Nat. Rev. Mol. Cell Biol. **2**:107–117.
16. **Somsel Rodman J, Wandinger-Ness A.** 2000. Rab GTPases coordinate endocytosis. J. Cell Sci. **113**:183–192.
17. **Smythe E.** 2002. Regulating the clathrin-coated vesicle cycle by AP2 subunit phosphorylation. Trends Cell Biol. **12**:352–354.
18. **Vonderheit A, Helenius A.** 2005. Rab7 associates with early endosomes to mediate sorting and transport of Semliki forest virus to late endosomes. PLoS Biol. **3**:e233. doi:10.1371/journal.pbio.0030233.
19. **Rink J, Ghigo E, Kalaidzidis Y, Zerial M.** 2005. Rab conversion as a mechanism of progression from early to late endosomes. Cell **122**:735–749.
20. **Gorvel JP, Chavrier P, Zerial M, Gruenberg J.** 1991. rab5 controls early endosome fusion in vitro. Cell **64**:915–925.
21. **Bucci C, Thomsen P, Nicoziani P, McCarthy J, van Deurs B.** 2000. Rab7: a key to lysosome biogenesis. Mol. Biol. Cell **11**:467–480.
22. **Lombardi D, Soldati T, Riederer MA, Goda Y, Zerial M, Pfeffer SR.** 1993. Rab9 functions in transport between late endosomes and the trans Golgi network. EMBO J. **12**:677–682.
23. **Ullrich O, Reinsch S, Urbe S, Zerial M, Parton RG.** 1996. Rab11 regulates recycling through the pericentriolar recycling endosome. J. Cell Biol. **135**:913–924.
24. **Urbe S, Huber LA, Zerial M, Tooze SA, Parton RG.** 1993. Rab11, a small GTPase associated with both constitutive and regulated secretory pathways in PC12 cells. FEBS Lett. **334**:175–182.
25. **Macovei A, Zitzmann N, Lazar C, Dwek RA, Branza-Nichita N.** 2006. Brefeldin A inhibits pestivirus release from infected cells, without affecting its assembly and infectivity. Biochem. Biophys. Res. Commun. **346**:1083–1090.
26. **Schulze A, Mills K, Weiss TS, Urban S.** 2012. Hepatocyte polarization is essential for the productive entry of the hepatitis B virus. Hepatology **55**:373–383.
27. **Lazar C, Durantel D, Macovei A, Zitzmann N, Zoulim F, Dwek RA, Branza-Nichita N.** 2007. Treatment of hepatitis B virus-infected cells with alpha-glucosidase inhibitors results in production of virions with altered molecular composition and infectivity. Antiviral Res. **76**:30–37.
28. **Krishnan MN, Sukumaran B, Pal U, Agaisse H, Murray JL, Hodge TW, Fikrig E.** 2007. Rab 5 is required for the cellular entry of dengue and West Nile viruses. J. Virol. **81**:4881–4885.
29. **Meertens L, Bertaux C, Dragic T.** 2006. Hepatitis C virus entry requires a critical postinternalization step and delivery to early endosomes via clathrin-coated vesicles. J. Virol. **80**:11571–11578.
30. **Sieczkarski SB, Whittaker GR.** 2003. Differential requirements of Rab5 and Rab7 for endocytosis of influenza and other enveloped viruses. Traffic **4**:333–343.
31. **Wolf M, Deal EM, Greenberg HB.** 2012. Rhesus rotavirus trafficking during entry into MA104 cells is restricted to the early endosome compartment. J. Virol. **86**:4009–4013.
32. **Lucifora J, Arzberger S, Durantel D, Belloni L, Strubin M, Levrero M, Zoulim F, Hantz O, Protzer U.** 2011. Hepatitis B virus X protein is essential to initiate and maintain virus replication after infection. J. Hepatol. **55**:996–1003.
33. **Zeigerer A, Gilleron J, Bogorad RL, Marsico G, Nonaka H, Seifert S, Epstein-Barash H, Kuchimanchi S, Peng CG, Ruda VM, Del Conte-Zerial P, Hengstler JG, Kalaidzidis Y, Koteliansky V, Zerial M.** 2012. Rab5 is necessary for the biogenesis of the endolysosomal system in vivo. Nature **485**:465–470.
34. **Maxfield FR, McGraw TE.** 2004. Endocytic recycling. Nat. Rev. Mol. Cell Biol. **5**:121–132.
35. **Ren M, Xu G, Zeng J, De Lemos-Chiarandini C, Adesnik M, Sabatini DD.** 1998. Hydrolysis of GTP on rab11 is required for the direct delivery of transferrin from the pericentriolar recycling compartment to the cell surface but not from sorting endosomes. Proc. Natl. Acad. Sci. U. S. A. **95**: 6187–6192.
36. **Vandenbulcke F, Nouel D, Vincent JP, Mazella J, Beaudet A.** 2000. Ligand-induced internalization of neurotensin in transfected COS-7 cells: differential intracellular trafficking of ligand and receptor. J. Cell Sci. **113**: 2963–2975.
37. **Trischler M, Stoorvogel W, Ullrich O.** 1999. Biochemical analysis of distinct Rab5- and Rab11-positive endosomes along the transferrin pathway. J. Cell Sci. **112**:4773–4783.
38. **Marsh M, Schmid S, Kern H, Harms E, Male P, Mellman I, Helenius A.** 1987. Rapid analytical and preparative isolation of functional endosomes by free flow electrophoresis. J. Cell Biol. **104**:875–886.
39. **Szymanski CJ, Humphries WH, IV, Payne CK.** 2011. Single particle tracking as a method to resolve differences in highly colocalized proteins. Analyst **136**:3527–3533.
40. **Wubbolts R, Fernandez-Borja M, Oomen L, Verwoerd D, Janssen H, Calafat J, Tulp A, Dusseljee S, Neefjes J.** 1996. Direct vesicular transport of MHC class II molecules from lysosomal structures to the cell surface. J. Cell Biol. **135**:611–622.
41. **Barbero P, Bittova L, Pfeffer SR.** 2002. Visualization of Rab9-mediated vesicle transport from endosomes to the trans-Golgi in living cells. J. Cell Biol. **156**:511–518.
42. **Lin SX, Mallet WG, Huang AY, Maxfield FR.** 2004. Endocytosed cation-independent mannose 6-phosphate receptor traffics via the endocytic recycling compartment en route to the trans-Golgi network and a subpopulation of late endosomes. Mol. Biol. Cell **15**:721–733.
43. **Ganley IG, Carroll K, Bittova L, Pfeffer S.** 2004. Rab9 GTPase regulates late endosome size and requires effector interaction for its stability. Mol. Biol. Cell **15**:5420–5430.
44. **Bridge AJ, Pebernard S, Ducraux A, Nicoulaz AL, Iggo R.** 2003. Induction of an interferon response by RNAi vectors in mammalian cells. Nat. Genet. **34**:263–264.
45. **Weaver DJ, Jr, Voss EW, Jr.** 1999. Kinetics and intracellular pathways required for major histocompatibility complex II-peptide loading and surface expression of a fluorescent hapten-protein conjugate in murine macrophage. Immunology **96**:557–568.
46. **Laurent-Matha V, Derocq D, Prebois C, Katunuma N, Liaudet-Coopman E.** 2006. Processing of human cathepsin D is independent of its catalytic function and auto-activation: involvement of cathepsins L and B. J. Biochem. **139**:363–371.
47. **Rigg RJ, Schaller H.** 1992. Duck hepatitis B virus infection of hepatocytes is not dependent on low pH. J. Virol. **66**:2829–2836.
48. **Collins DS, Unanue ER, Harding CV.** 1991. Reduction of disulfide bonds within lysosomes is a key step in antigen processing. J. Immunol. **147**: 4054–4059.
49. **Sinnathamby G, Maric M, Cresswell P, Eisenlohr LC.** 2004. Differential requirements for endosomal reduction in the presentation of two H2-E^d-

restricted epitopes from influenza hemagglutinin. J. Immunol. **172**:6607–6614.
50. **Hayer A, Stoeber M, Ritz D, Engel S, Meyer HH, Helenius A.** 2010. Caveolin-1 is ubiquitinated and targeted to intralumenal vesicles in endolysosomes for degradation. J. Cell Biol. **191**:615–629.
51. **Modis Y, Ogata S, Clements D, Harrison SC.** 2004. Structure of the dengue virus envelope protein after membrane fusion. Nature **427**:313–319.
52. **Smith AE, Helenius A.** 2004. How viruses enter animal cells. Science **304**:237–242.
53. **Kim C, Bergelson JM.** 2012. Echovirus 7 entry into polarized intestinal epithelial cells requires clathrin and Rab7. mBio **3**(2):e00304-11. doi:10.1128/mBio.00304-11.
54. **Mannova P, Forstova J.** 2003. Mouse polyomavirus utilizes recycling endosomes for a traffic pathway independent of COPI vesicle transport. J. Virol. **77**:1672–1681.
55. **Suikkanen S, Saajarvi K, Hirsimaki J, Valilehto O, Reunanen H, Vihinen-Ranta M, Vuento M.** 2002. Role of recycling endosomes and lysosomes in dynein-dependent entry of canine parvovirus. J. Virol. **76**:4401–4411.
56. **Mangold CM, Streeck RE.** 1993. Mutational analysis of the cysteine residues in the hepatitis B virus small envelope protein. J. Virol. **67**:4588–4597.
57. **Feener EP, Shen WC, Ryser HJ.** 1990. Cleavage of disulfide bonds in endocytosed macromolecules. A processing not associated with lysosomes or endosomes. J. Biol. Chem. **265**:18780–18785.
58. **Ohgami RS, Campagna DR, Greer EL, Antiochos B, McDonald A, Chen J, Sharp JJ, Fujiwara Y, Barker JE, Fleming MD.** 2005. Identification of a ferrireductase required for efficient transferrin-dependent iron uptake in erythroid cells. Nat. Genet. **37**:1264–1269.
59. **Yang J, Chen H, Vlahov IR, Cheng JX, Low PS.** 2006. Evaluation of disulfide reduction during receptor-mediated endocytosis by using FRET imaging. Proc. Natl. Acad. Sci. U. S. A. **103**:13872–13877.
60. **Fenouillet E, Barbouche R, Jones IM.** 2007. Cell entry by enveloped viruses: redox considerations for HIV and SARS-coronavirus. Antioxid. Redox Signal. **9**:1009–1034.
61. **Ryser HJ, Fluckiger R.** 2005. Progress in targeting HIV-1 entry. Drug Discov. Today **10**:1085–1094.
62. **Abou-Jaoude G, Sureau C.** 2007. Entry of hepatitis delta virus requires the conserved cysteine residues of the hepatitis B virus envelope protein antigenic loop and is blocked by inhibitors of thiol-disulfide exchange. J. Virol. **81**:13057–13066.
63. **Sokolowska I, Dorobantu C, Woods AG, Macovei A, Branza-Nichita N, Darie CC.** 2012. Proteomic analysis of plasma membranes isolated from undifferentiated and differentiated HepaRG cells. Proteome Sci. **10**:47.
64. **Hao X, Shang X, Wu J, Shan Y, Cai M, Jiang J, Huang Z, Tang Z, Wang H.** 2011. Single-particle tracking of hepatitis B virus-like vesicle entry into cells. Small **7**:1212–1218.
65. **Lambert C, Thome N, Kluck CJ, Prange R.** 2004. Functional incorporation of green fluorescent protein into hepatitis B virus envelope particles. Virology **330**:158–167.
66. **Fredericksen BL, Wei BL, Yao J, Luo T, Garcia JV.** 2002. Inhibition of endosomal/lysosomal degradation increases the infectivity of human immunodeficiency virus. J. Virol. **76**:11440–11446.
67. **Cooper A, Shaul Y.** 2006. Clathrin-mediated endocytosis and lysosomal cleavage of hepatitis B virus capsid-like core particles. J. Biol. Chem. **281**:16563–16569.